ACS APPLIED MATERIALS & INTERFACES

Research Article

www.acsami.org

All-Nano-TiO_2 Compact Film for High-Performance Dye-Sensitized Solar Cells

Kassio P. S. Zanoni, Ronaldo C. Amaral, and Neyde Y. Murakami Iha*

Laboratory of Photochemistry and Energy Conversion, Departamento de Química Fundamental, Instituto de Química, Universidade de São Paulo-USP, Av. Prof. Lineu Prestes, 748, 05508-000 São Paulo, SP, Brazil

Supporting Information

ABSTRACT: An innovative all-nano-TiO_2 thin film capable of enhancing dye-sensitized solar cell (DSC) photoefficiencies was prepared by a layer-by-layer method beneath the meso-TiO_2 film, employing acid and basic nano-TiO_2 sols as cations and anions, respectively. TiO_2 syntheses were performed under absolute control to lead to appropriate morphological and optical properties to yield high-quality compact films using profilometry, tuning, and scanning electron microscopy. A detailed study by photoelectrochemical parameters, incident photon-to-current efficiency, electron lifetime, and electrochemical impedance spectroscopy demonstrates that the physical contact between FTO and the electrolyte is prevented and the role of the compact film has been elucidated. DSCs with TiO_2 bilayers on top of FTO improved the conversion efficiency up to 62%, mainly because of the prevention of FTO/I_3^- charge recombination and an improved contact between FTO and TiO_2.

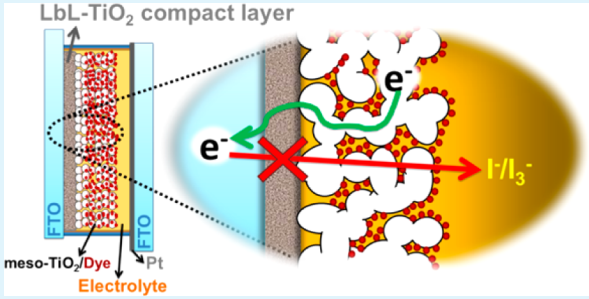

KEYWORDS: *dye-sensitized solar cells, compact layer, blocking layer, charge recombination prevention, TiO_2 thin film, layer-by-layer*

INTRODUCTION

New materials and components have been intensively developed to improve dye-sensitized solar cells (DSCs). In particular, the engineering of photoanodes has provided some innovative approaches.[1−18]

Intensive efforts have been focused to prevent charge recombination at meso-TiO_2/electrolyte and FTO/electrolyte interfaces to avoid back reactions of photoinjected electrons with I_3^- species.[19−25] Several attempts have been made to improve DSC performance, but the most efficient approach is the application of a compact layer on FTO or meso-TiO_2 surfaces by using different methods and materials. Blocking layers at the meso-TiO_2/electrolyte interface are mainly fabricated by employing Nb_2O_5, $SrTiO_3$, and/or Al_2O_3 thin films,[26,27] while the prevention of physical contact between FTO and the electrolyte is achieved by immersion in oxide precursor solutions, such as $TiCl_4$ dissolved in an ice/water mixture, spray pyrolysis, spin-coating, sputtering, and layer-by-layer or chemical vapor deposition.[23,26−40]

In our previous work, we have demonstrated that DSC efficiencies can be improved by incorporation of layer-by-layer (LbL) self-assembled films.[28,30,33,34] In particular, the LbL technique is a low-cost procedure for thin film deposition that offers rigorous control of morphology and the possibility of scaling up and can be employed to assemble almost all classes of materials, such as polymers, organic dyes, colloidal particles, graphene, carbon nanotubes, quantum dots, proteins, enzymes, and DNA.[41−43] Our first approach started with TiO_2 nanoparticles as cations paired with polyelectrolytes as anions, such as sodium-sulfonated polystyrene (PSS), sulfonated lignin (SL), and poly(acrylic acid) (PAA).[33,34] When deposited on the FTO surface, these compact films work as blocking and contact layers, which decrease the extent of electron recombination and improve the contact between the meso-TiO_2 and FTO.[33] However, the choice of the appropriate oppositely charged organic polymer paired with TiO_2 is a difficult task, because most of the polyelectrolytes are not thermally stable at the TiO_2 sintering temperature (500 °C). Thus, we developed an innovative LbL film made solely with TiO_2, for which positively and negatively charged TiO_2 nanoparticles were obtained by two different routes, acidic and basic ones, respectively.[30] We further developed the high-performance compact film in this work following our ongoing efforts to improve the quality of this film to exceed our previous results. A morphological characterization has been further performed using profilometry, tuning, and scanning electron microscopy. Here, we also include a detailed study of photoelectrochemical features of DSCs having LbL TiO_2 only films beneath the meso-TiO_2 layer to elucidate and certify the role of the compact film as a very effective contact and blocking layer.

EXPERIMENTAL SECTION

Synthesis of TiO_2 Nanoparticles. TiO_2 nanoparticles were prepared by the sol−gel method employing acid and basic hydrolysis conditions, as detailed previously.[30,33,34,44] In the acid route, 24 mL of

Received: March 31, 2014
Accepted: June 4, 2014
Published: June 4, 2014

Scheme 1. Assembly of All-Nano-TiO_2 Compact Films Using Oppositely Charged Nanoparticle TiO_2 by the LbL Techinique

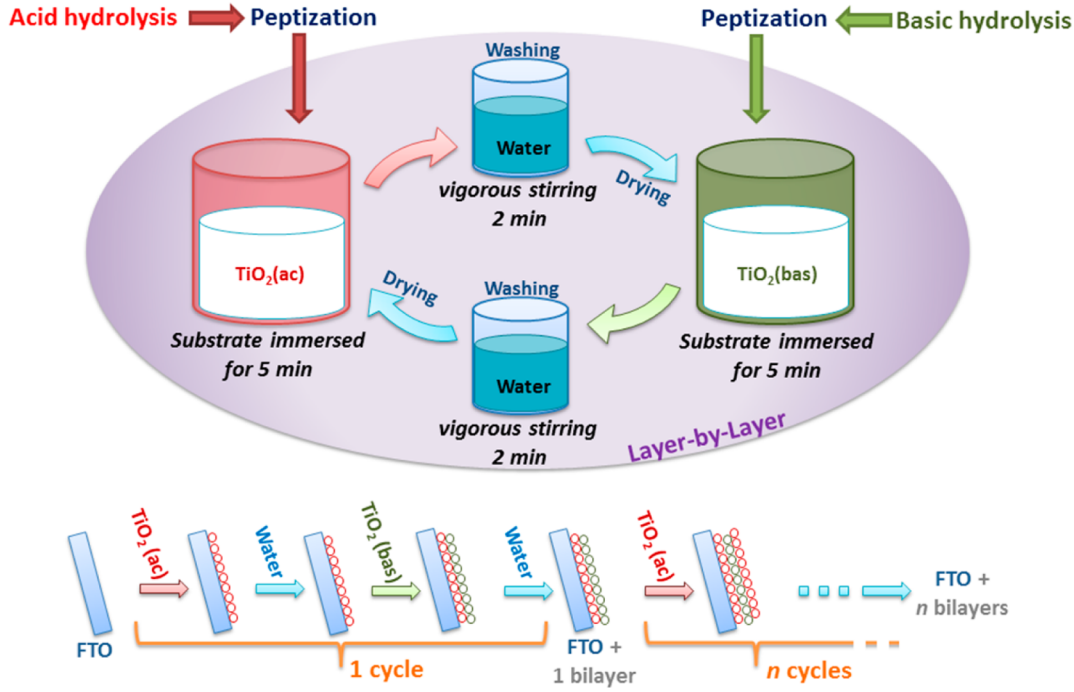

titanium(IV) isopropoxide (Sigma-Aldrich) was added dropwise to 140 mL of an aqueous 0.1 mol L^{-1} HNO_3 solution that was being vigorously stirred. In basic hydrolysis, the same volume of titanium-(IV) isopropoxide was slowly dropped into 140 mL of an aqueous 0.1 mol L^{-1} ammonia solution in an ice bath. In the following peptization step, both acid and basic sols were stirred and heated (80 °C) for 8 h, resulting in nanoparticles named TiO_2(ac) and TiO_2(bas), respectively.

Deposition of a Compact TiO_2 Film by the LbL Technique. TiO_2(ac) and TiO_2(bas) were used as cations and anions, respectively, for deposition of compact films by the LbL method on top of the FTO surface, named LbL-TiO_2/FTO hereafter (Scheme 1).

A precleaned FTO substrate (Pilkington, TEC-15, 15 Ω/□) was immersed alternately in nonautoclaved suspensions of TiO_2(ac) (25 mg mL^{-1}, pH 2) and TiO_2(bas) (5 mg mL^{-1}, pH ~10) for 5 min. Each immersion was followed by washing and drying in cycles to produce 7, 15, 22, or 30 bilayers on the surface of the FTO.

Assembly of DSCs. A meso-TiO_2 paste (Dyesol) was deposited by an ATMA AT25PA screen printer or painting directly over bare FTO substrates and on LbL-TiO_2/FTO and sintered at 500 °C for 30 min. Its sensitization was achieved by the immersion of electrodes in a saturated ethanolic solution of N719 (Dyesol), *cis*-[Ru-$(dcbH)_2(NCS)_2$][TBA]$_2$ (dcbH = 2,2′-bipyridyl-4,4′-dicarboxylate, and TBA = tetrabutylammonium). The adsorbed dye concentration was determined spectrophotometrically by desorption with an aqueous 10^{-4} mol L^{-1} NaOH solution. Photoanodes with or without TiO_2 compact bilayers were assembled in a sandwich-type arrangement (Figure 1) using Pt-covered FTO as counter electrodes.[30,44] Counter electrode sheets had holes previously drilled using a Comco Inc. AccuFlo microabrasive blaster for insertion of the electrolyte inside cells. Electrolyte solutions consisted of 0.005 mol L^{-1} I_2, 0.5 mol L^{-1} LiI, and 0.5 mol L^{-1} pyridine in acetonitrile and 3-methyl-2-oxazolidinone [9:1 (v/v)] or Electrolyte EL-HTE (Dyesol). Cells were sealed with a polymer-based hot melt foil, Surlyn (DuPont), using a hot press homemade machine that consisted of a Watlow EZ-ZONE temperature controller and a Watlow Ultramic ceramic heater.

Surface Characterization. Surface parameters, such as thickness, roughness, and waviness, were obtained by employing a KLA Tencor P-6 profilometer. Because a typical surface profile exhibits roughness superimposed over waviness, deviations in waviness were factored out of the raw profile data in Profiler version 7.35 by employing a 0.14 μm

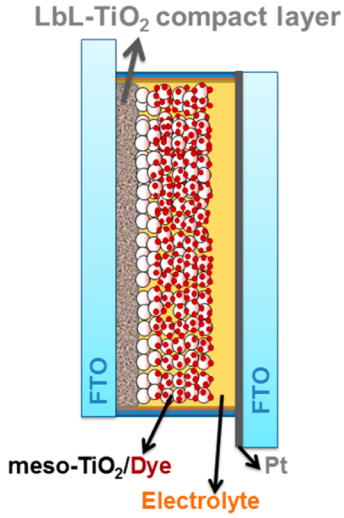

Figure 1. All-nano-TiO_2 compact film deposited on the FTO surface beneath the mesoporous layer in a DSC assemblage.

low pass algorithmic filter that best fit to the investigated sample. TiO_2 nanoparticle sizes were evaluated by transmission electron microscopy (TEM) using a JEOL 2010F-FasTEM microscope with an accelerating voltage of 200 kV. The surface morphology of FTO and TiO_2 layers was characterized by scanning electron microscopy in a Hitachi S-4700 Cold Cathode Field Emission SE Microscope, with an accelerating voltage of 2 kV.

DSC Photoelectrochemical Characterization. Photocurrent–photovoltage curves (J–V curves) and the open circuit voltage decay (OCVD) were recorded with a Gamry 500 or Gamry Interface 1000 potentiostat at a simulated solar radiation (~100 mW cm^{-2}) provided by Newport solar simulators (AM 1.5 filter), as previously described.[11,45] The photoelectrochemical results are averages of, at least, four individual cells. Electrochemical impedance (EI) spectra of illuminated DSCs were recorded with a Gamry 500 or Interface 1000 potentiostat over a frequency range of 5×10^{-1} to 10^5 Hz under a 10 mV ac amplitude signal. Data were analyzed using Gamry Echem

dx.doi.org/10.1021/am501955f | ACS Appl. Mater. Interfaces 2014, 6, 10421–10428

Scheme 2. Acid- or Base-Promoted Hydrolysis of Ti(IV) Isopropoxide and Its Subsequent Condensation Step

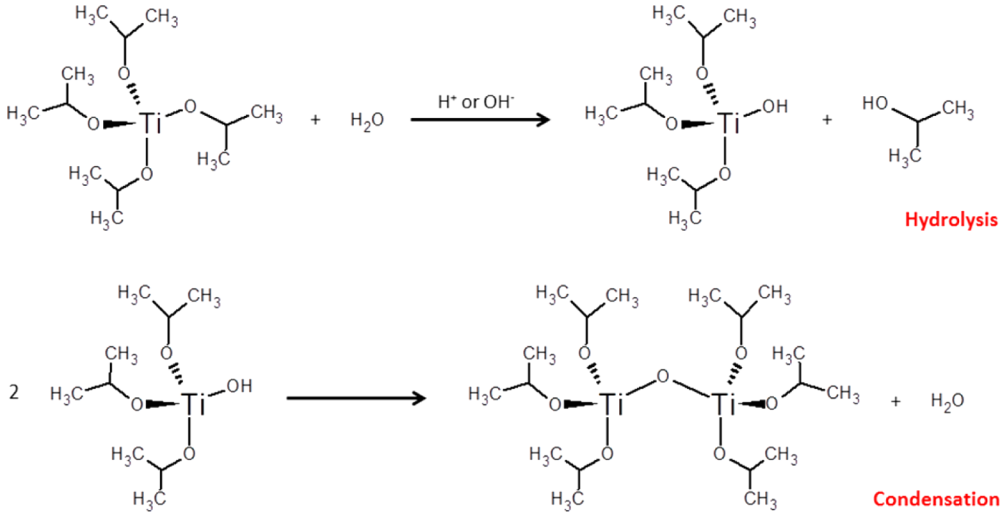

analyst software. Incident photon-to-current efficiency (IPCE) spectra were measured using an Oriel system comprised by a 400 W Xe lamp coupled to a 0.25 m Czerny-Turner monochromator, described previously,[46] or an Oriel 6251 75 W Xe lamp coupled with a Cornerstone 260 monochromator.

RESULTS AND DISCUSSION

Microscopic and Morphological Characterization. Acid- or base-promoted hydrolysis of Ti(IV) isopropoxide and its subsequent condensation step leads to three-dimensional polymeric Ti−O−Ti chains[40,47,48] as shown in Scheme 2. Thus, dropwise addition of the titanium precursor guarantees a very high water/titanium ratio and leads to a negligible kinetic effect of the hydrolysis step.[40] Depending on experimental conditions, such as pH, temperature, condensing agents, and/or templates, continuous hydrolysis will lead to the precipitation of aggregates and particles with different shapes and sizes.[47] Therefore, here, we adopted a rigorous control of the synthesis conditions, in particular temperature, to achieve optimization of the optical and morphological characteristics of the nanoparticle.

Acid hydrolysis results in a translucent TiO_2(ac) sol, visually better dispersed than the opaque TiO_2(bas) sol,[40] because in the nanoparticle formation step of the acid route, superficial Ti−OH sites are constantly protonated, which decreases the condensation rate, yielding small particles (~4 nm in diameter) as indicated in TEM micrographs (Figure S1 of the Supporting Information). On the other hand, the basic hydrolysis shifts the superficial Ti−OH ⇌ Ti−O^- + H^+ equilibrium to the dissociated form, which facilitates condensation.[30] The resulting singular nanoparticles are as small as the acid ones (~3 nm), and occasional agglomerates were destroyed and dispersed into primary particles in the following peptization step. This stage also needs the rigorous control of the temperature and pH becoming easier as the pH values deviate from the isoelectric point (pH 7).[40] The so obtained optimized acidic and basic TiO_2 sols (pH ~2 and ~10, respectively) were assembled into TiO_2 bilayers by the LbL technique, as shown in Scheme 1.

Scanning electron micrographs of LbL films (Figure 2) show a very thin, compact nanostructure, drastically differing from the mesoscopic morphology of the meso-TiO_2 film. The number of TiO_2 bilayers is linear with respect to the thickness of the film, being 30 bilayers around 120 nm and 7 bilayers

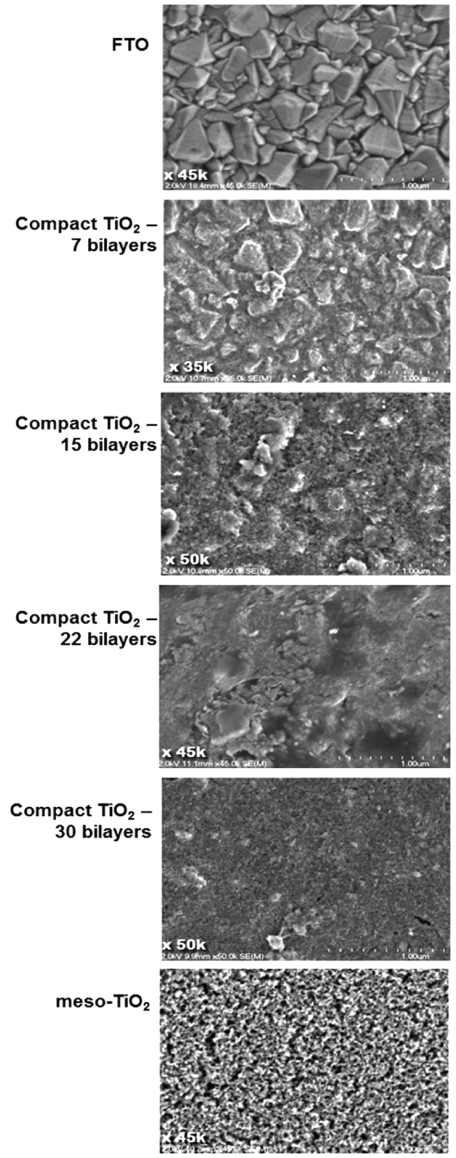

Figure 2. Surface SEM micrographs of LbL-TiO_2/FTO and meso-TiO_2/FTO after sinterization.

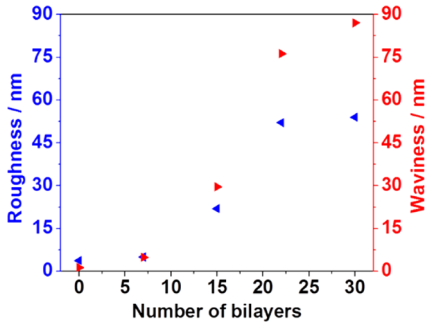

Figure 3. Surface roughness (blue triangles) and waviness (red triangles) of LbL-TiO_2/FTO.

around 30 nm (Table S1 of the Supporting Information). TiO_2 compact films with 22 and 30 bilayers effectively cover the FTO surface, while the 7-bilayer film is not thick enough, leading to a similar surface pattern of a bare FTO due to exposed conducting oxide particles.

A comparison of their surface roughness and waviness (Figure 3) corroborates the observation described above with a clear indication that samples with seven bilayers have basically FTO surface morphology, while thicker films (i.e., 22 and 30 bilayers) possess characteristics of the TiO_2 compact film that cover the conducting oxide, reaching constant waviness and roughness values after ~20 bilayers. Cross-section SEM micrographs (Figure S3 of the Supporting Information) show enhanced contact between compact TiO_2 and FTO particles.

Optical Properties of LbL-Modified Photoanodes. LbL-TiO_2/FTO substrates show a decrease in transmittance at 540 nm (maximum of the N719 injection band) as the number of bilayers increases (Figure S4 of the Supporting Information). Sintered LbL-TiO_2/FTO and meso-TiO_2/FTO substrates were left immersed in an N719 dye solution overnight. While the meso-TiO_2 film became purple after a few minutes because of dye adsorption, no color was observed with bare eyes for the TiO_2 compact films. The adsorbed dye spectroscopically determined after desorption with aqueous 10^{-4} M NaOH is 9.8×10^{-8} mol cm^{-2} for meso-TiO_2/FTO and $\sim 0.2 \times 10^{-8}$ mol cm^{-2} for LbL-TiO_2/FTO. Therefore, TiO_2 underlayers do not contribute to the light harvesting of photoanodes due to the negligible dye absorption by the compact film.

Photoelectrochemical Characterization of DSCs. Photoelectrochemical parameters of N719-sensitized solar cells with and without TiO_2 compact layers are listed in Table 1. Experimentally obtained maximal efficiencies, global efficiencies (η_g), were corrected by the decrease in substrate transmittance, named corrected efficiencies (η_c), which represent the actual electronic collection effectiveness. Figure 4A pictures their so

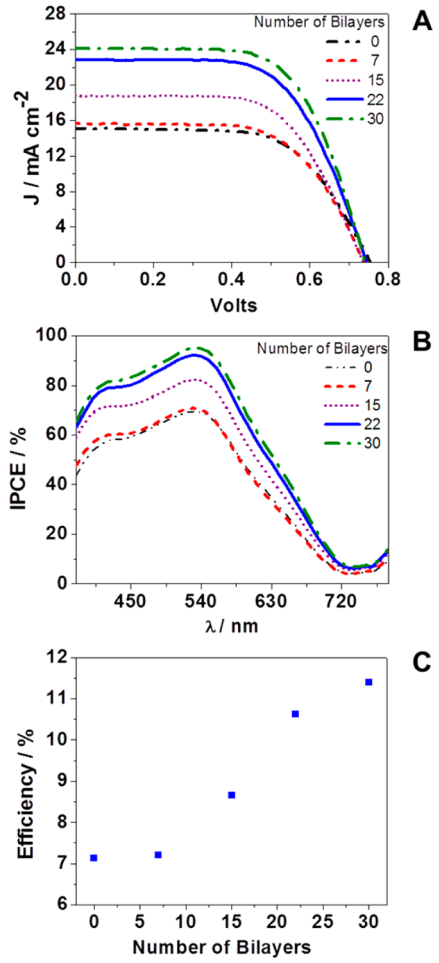

Figure 4. Photoelectrochemical characterization of N719-sensitized DSCs with TiO_2 compact bilayers on the surface of FTO, beneath the mesoporous TiO_2 layer. (A) Corrected current–voltage curves (~100 mW cm^{-2}, AM 1.5). (B) Corrected incident photon to current efficiency spectra. (C) Improvements in electron collection efficiency (η_c) vs the number of bilayers. Results are averages of at least four individual cells.

corrected J–V curves, while corrected efficiency improvements as a function of the number of bilayers are shown in Figure 4B.

DSCs assembled using compact TiO_2 underlayers exhibit remarkably high efficiencies, and the best η_g, without correction by the transmittance loss, is found for 22 compact bilayers (8.36%, 17% improvement). Enhanced η_g values are mainly due to better short-circuit current densities (J_{SC}), because open-circuit voltages (V_{OC}) are slightly smaller than those of devices without compact films. J_{SC} and, consequently, η_g are similar between zero and seven bilayers, and they substantially increase

Table 1. Photoelectrochemical Parameters for N719-Sensitized DSCs as a Function of the Number of TiO_2 Compact Bilayers on FTO beneath the Mesoporous TiO_2 Layer (~100 mW cm^{-2}, AM 1.5)[a]

no. of bilayers	$T_{540\ nm}$ (%)	J_{SC} (mA cm^{-2})	V_{oc} (V)	ff	η_g (%)	η_c (%)	efficiency improvement[b] (%)
0	100	15.2 ± 0.7	0.75 ± 0.01	0.62 ± 0.02	7.12 ± 0.26	7.12	0
7	98	15.3 ± 0.9	0.74 ± 0.01	0.62 ± 0.03	7.06 ± 0.33	7.20	1.1
15	89	16.7 ± 0.8	0.74 ± 0.01	0.63 ± 0.02	7.71 ± 0.27	8.66	22
22	79	18.0 ± 0.9	0.74 ± 0.02	0.62 ± 0.03	8.36 ± 0.57	10.6	49
30	68	16.4 ± 0.9	0.74 ± 0.01	0.64 ± 0.04	7.80 ± 0.36	11.5	62

[a]Results are averages of at least four individual cells. [b]Compared to DSC without a LbL-TiO_2 film.

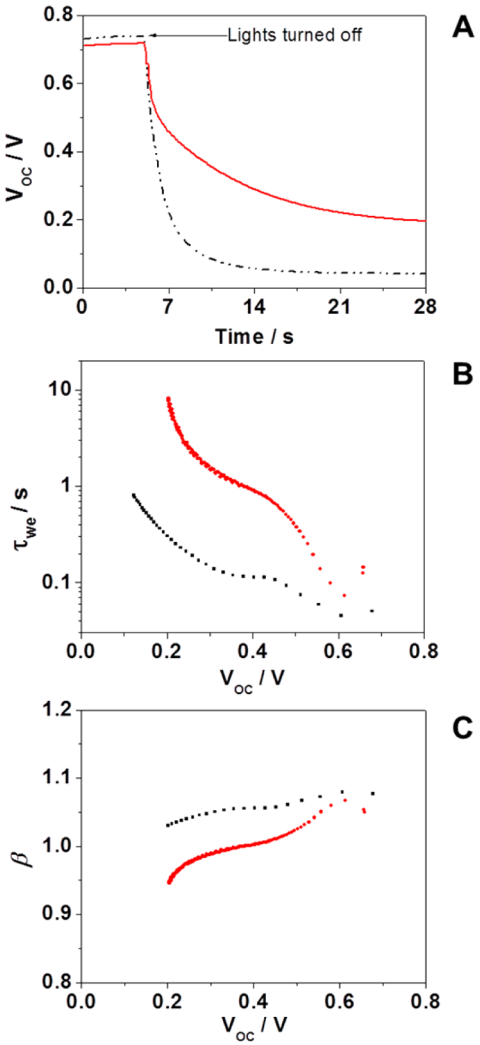

Figure 5. Open circuit voltage decays (A), electron lifetimes (B), and recombination parameters (C) of N719-sensitized DSCs with (red) or without (black) 22 bilayers of the compact TiO_2 film.

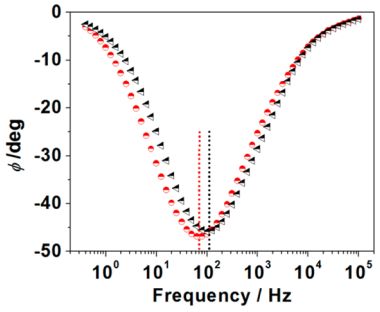

Figure 6. Bode plot of LbL-TiO_2/FTO (red) or bare FTO (black) substrates under open-circuit conditions.

until they reach maximal values at 22 bilayers. An apparent decrease in J_{SC} (from 18.0 to 16.4 mA cm^{-2}) with a consequent decrease in η_g (from 8.36 to 7.80%) observed for the 30-bilayer sample is a result of a decreased level of uptake of light caused by a considerably lower transmittance of the thicker LbL-TiO_2/FTO substrate. Taking in account only the electron collection efficiency by correction of the transmittance loss, we found the 22-bilayer film leads to an enhancement of 49% in η_c, being exceeded by only that of the 30-bilayer film, with an impressive

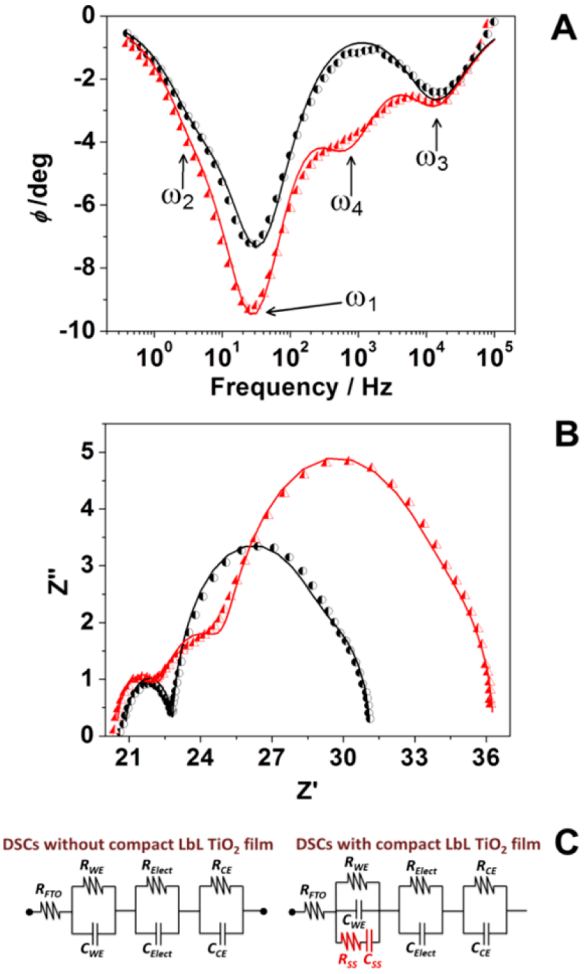

Figure 7. Bode (A) and Nyquist (B) plots of illuminated N719-sensitized DSCs with (red) or without (black) compact TiO_2 bilayers under open-circuit conditions. The lines in panels A and B are the fits obtained using the equivalent circuits shown in panel C.

62% improvement. Higher η_c values are in accordance with higher corrected incident photon-to-current efficiency (IPCE) spectra (Figure 4B), as a consequence of FTO/TiO_2 contact enhancement, and charge recombination prevention.[35,49] Improvements in current and IPCE are remarkably higher than in our previous works using TiO_2/Nb_2O_5 compact bilayers,[28] and efficiencies exceeded those of DSCs with TiO_2/PSS bilayers[33,34] and with the TiO_2 compact film of our preliminary study.[30]

The similarity between Figures 3 and 4C points to a correlation of the surface microscopic morphology of compact layers and cell efficiencies. In fact, a 1.1% improvement is observed for DSCs with 7 bilayers, for which surface characterization indicates exposed FTO particles, while remarkable enhancements are observed by employing 22 and 30 bilayers, in which FTO is perfectly covered by the TiO_2 compact layer. Therefore, the electron collection efficacy at the FTO is enhanced by the rougher surface as a consequence of an increased contact between TiO_2 and FTO, which is promoted by the sintering step.

Open-circuit voltage decays (OCVDs) of DSCs with and without LbL-TiO_2 bilayers (Figure 5A) were obtained, and their electron lifetimes (τ_{WE}), which are the characteristic times of recovery after the system is displaced from the OC

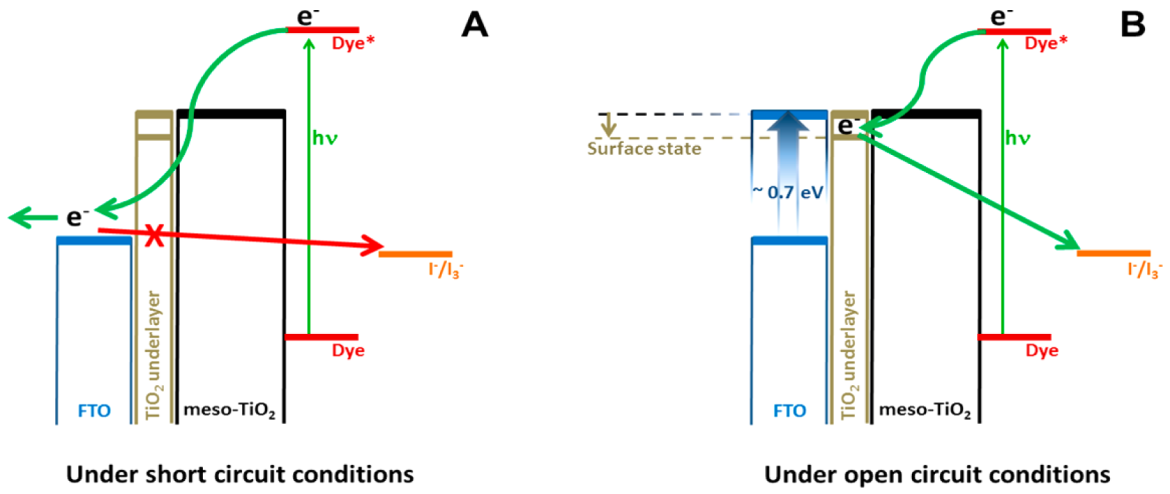

Figure 8. Role of blocking TiO_2 underlayers under short-circuit (A) and open-circuit (B) conditions.

condition,[29,35,50] were calculated using eq 1 (Figure 5B) to evaluate the extent of charge recombination.

$$\tau_{WE} = -\frac{k_B T}{e}\left(\frac{dV_{OC}}{dt}\right)^{-1} \quad (1)$$

k_B is Boltzmann's constant, e the elementary charge, T the temperature in kelvin, and dV_{OC}/dt the derivative of the open-circuit voltage decay.

DSCs with TiO_2 compact bilayers exhibit τ_{WE} values 10-fold longer than the values of those without it, because of the drastic decrease in the level of electron recombination.[29,35,50] The electron lifetime can also be calculated from eq 2, where n is the free electron density in the TiO_2 nanostructure and $U(n)$ is the recombination rate that is dependent on n (eq 3).[50]

$$\tau_{WE} = \frac{n}{U(n)} \quad (2)$$

$$U(n) = k_r n^{\beta} \quad (3)$$

The recombination rate mediated by the electron acceptor I_3^- is nonlinear (eq 3), where β is the recombination parameter or effective recombination order (Figure 5C) that gives a profile of the lifetime dependence on the V_{OC} of DSCs.[50] From eqs 1−3, β can be also calculated by eq 4.

$$\beta = 1 + \frac{k_B T}{e}\left[\frac{\partial \ln(\tau_{WE}^{-1})}{\partial V_{OC}}\right] \quad (4)$$

β is usually constant and ∼1, as shown in Figure 5C with lower effective recombination orders for devices with compact TiO_2 underlayers as a direct consequence of a decreased recombination rate.

Electrochemical impedance spectroscopy (EIS) supports the discussion presented above about the blocking layer effect. A comparison of EI spectra of LbL-TiO_2/FTO and bare FTO substrates, without meso-TiO_2/dye, can be observed in Figure 6. These substrates were set as working electrodes with platinized FTO substrates as the counter electrode, and measurements were performed in the presence of the same I^-/I_3^- electrolyte, under open-circuit conditions. The intense phase angle peak around 1.1×10^2 Hz (Figure 6) is mainly ascribed to charge exchange between the working electrode and electrolyte.[23,51−53] In addition, processes from counter electrode/electrolyte charge transfer and electrolyte diffusion can be observed around 1×10^4 Hz and $3 \times 10°$, respectively,[33,52] although not clearly in EI spectra because of an overlap with the intense signal. Unfortunately, these signal overlaps avoid an accurate fit of an equivalent circuit model to the observed EI spectra as well as a quantitative description. In spite of this, qualitative analyses indicate that the main phase angle peak shifts to lower frequencies, ∼7.0 × 10 Hz, for LbL-TiO_2/FTO due to the decrease in the recombination rate at the FTO/electrolyte interface. When this is set up on DSCs, the so effectively enhanced electron lifetime can be observed in Figure 5B, in which the inhibition of FTO/electrolyte back reactions is clear for any bias < OC.

EI spectra for DSCs, with meso-TiO_2/dye, under OC conditions are shown in Figure 7A. For both samples, a main phase angle peak is observed around 3 × 10 Hz, named ω_1, and ascribed to charge transfer processes across the working electrode/electrolyte interface.[23,51−53] Diffusion within the electrolyte, named ω_2, and electron exchanges across the electrolyte/counter electrode interface, named ω_3, are around $2 \times 10°$ and 2×10^4 Hz, respectively, and just slightly overlapped with ω_1.

The appearance of a new signal around 1×10^3 Hz, named ω_4, is observed after introduction of TiO_2 underlayers and ascribed to the nonideal interface between electrolyte and TiO_2 compact films, with surface states that arise from interactions between the TiO_2 surface and components of the electrolyte as suggested by Cameron et al.[23] In addition to the appearance of ω_4, an enhancement of ω_1 resistance is observed (from 6.15 to 11.6 Ω cm^{-2}, as shown in Table S2 of the Supporting Information). Both features are a consequence of a smaller diffusion rate within the semiconductor[52] causing current losses due to a faster rate of recombination of trapped electrons at the surface state.[23] In other words, although the back reaction from FTO is prevented under any bias < OC, charge recombination from the surface state has a major role in DSCs with a LbL compact layer under open-circuit conditions. The slightly lower V_{OC} is a consequence of these effects, which also lead to a smaller dark current (Figure S5 of the Supporting Information). Figure 8 summarizes the role of blocking TiO_2 underlayers under short- and open-circuit conditions.

Under short-circuit conditions (Figure 8A), the FTO Fermi level is close to the redox one, as a consequence of a rapid electron transfer at the counter electrode.[23] Under this

condition or at any applied voltage lower than the open-circuit voltage, the TiO_2 underlayer acts as a physical barrier that prevents charge recombination from FTO. Under open-circuit conditions, the FTO Fermi level rises by ~0.7 eV, pairing with the TiO_2 Femi level,[23,52] and back reactions are favored, in particular via the compact TiO_2 surface state, which lead to slightly smaller V_{OC} values for LbL-TiO_2 DSCs.

CONCLUSION

The high-performance compact films prepared by LbL using solely TiO_2 nanoparticles effectively work as FTO/TiO_2 contact and FTO/electrolyte blocking layers under short-circuit conditions, which leads to an impressive 62% improvement in DSC efficiencies. A complete elucidation by photoelectrochemical parameters, IPCE, τ_{WE}, and EI spectra shows that the physical contact between FTO and the electrolyte is prevented and, consequently, electrons can survive longer without undergoing losses by coupled reactions at the FTO/electrolyte interface at any bias < OC. Under open-circuit conditions, the charge recombination from the compact TiO_2 surface states has a major role and leads to a slightly lower V_{OC}.

The simplicity of the cell design, including an affordable fabrication process, as well as the respectable and reproducible efficiency enhancement, promises a significant reduction of solar energy production costs. Moreover, the optical and morphological characteristics of the LbL-TiO_2 film, such as enhanced FTO/TiO_2 interaction and compact nanostructure, open up new applications not only in DSC photoanodes but also as antireflection self-cleaning materials, electrode surface protectors, and contact enhancers in different molecular devices, e.g., dye-sensitized photoelectrosynthesis cells.

ASSOCIATED CONTENT

Supporting Information

Transmission and scanning electron micrographs, transmittance and energy dispersive X-ray spectra of LbL-TiO_2/FTO, dark current−voltage curves, and electrochemical parameters obtained from EIS fits. This material is available free of charge via the Internet at http://pubs.acs.org.

AUTHOR INFORMATION

Corresponding Author

*E-mail: neydeiha@iq.usp.br.

Notes

The authors declare no competing financial interest.

ACKNOWLEDGMENTS

This work was supported by Fundação de Amparo à Pesquisa do Estado de São Paulo (FAPESP) and Conselho Nacional de Desenvolvimento Científico e Tecnológico (CNPq/CTEnerg). We thank Bruna K. Kariyazaki and Danilo R. M. Barbosa for general assistance, Dr. Amar S. Khumbar and the Chapel Hill Analytical and Nanofabrication Laboratory (CHANL, Chapel Hill, NC) for microscopy analyses, and Dr. Thomas J. Meyer and the Department of Chemistry of the University of North Carolina at Chapel Hill (Chapel Hill, NC) for some instrumental facilities.

REFERENCES

(1) Ye, M.; Zheng, D.; Wang, M.; Chen, C.; Liao, W.; Lin, C.; Lin, Z. Hierarchically Structured Microspheres for High-Efficiency Rutile TiO_2-Based Dye-Sensitized Solar Cells. *ACS Appl. Mater. Interfaces* **2014**, *6*, 2893−2901.

(2) Xie, F.; Cherng, S.-J.; Lu, S.; Chang, Y.-H.; Sha, W. E. .I; Feng, S.-P.; Chen, C.-M.; Choy, W. C. H. The Functions of Self-assembled Ultrafine TiO_2 Nanocrystals for High Efficient Dye-Sensitized Solar Cells. *ACS Appl. Mater. Interfaces* **2014**, *6*, 5367−5373.

(3) Chandiran, A. K.; Yella, A.; Stefik, M.; Heiniger, L.-P.; Comte, P.; Nazeeruddin, M. K.; Grätzel, M. Low-Temperature Crystalline Titanium Dioxide by Atomic Layer Deposition for Dye-Sensitized Solar Cells. *ACS Appl. Mater. Interfaces* **2013**, *5*, 3487−3493.

(4) Chu, F.; Li, W.; Shi, C.; Liu, E.; He, C.; Li, J.; Zhao, N. Performance Improvement of Dye-Sensitized Solar Cells Using Room-Temperature-Synthesized Hierarchical TiO_2 Honeycomb Nanostructures. *ACS Appl. Mater. Interfaces* **2013**, *5*, 7170−7175.

(5) Ahn, J. Y.; Moon, K. J.; Kim, J. H.; Lee, S. H.; Kang, J. W.; Lee, H. W.; Kim, S. H. Designed Synthesis and Stacking Architecture of Solid and Mesoporous TiO_2 Nanoparticles for Enhancing the Light-Harvesting Efficiency of Dye-Sensitized Solar Cells. *ACS Appl. Mater. Interfaces* **2014**, *6*, 903−909.

(6) Hagfeldt, A.; Boschloo, G.; Sun, L.; Kloo, L.; Pettersson, H. Dye-Sensitized Solar Cells. *Chem. Rev.* **2010**, *110*, 6595−6663.

(7) Lü, X.; Mou, X.; Wu, J.; Zhang, D.; Zhang, L.; Huang, F.; Xu, F.; Huang, S. Improved-Performance Dye-Sensitized Solar Cells Using Nb-Doped TiO_2 Electrodes: Efficient Electron Injection and Transfer. *Adv. Funct. Mater.* **2010**, *20*, 509−515.

(8) Heng, L.; Wang, X.; Yang, N.; Zhai, J.; Wan, M.; Jiang, L. p−n-Junction-Based Flexible Dye-Sensitized Solar Cells. *Adv. Funct. Mater.* **2010**, *20*, 266−271.

(9) Zakeeruddin, S. M.; Grätzel, M. Solvent-Free Ionic Liquid Electrolytes for Mesoscopic Dye-Sensitized Solar Cells. *Adv. Funct. Mater.* **2009**, *19*, 2187−2202.

(10) Zhang, Y.; Xie, Z.; Wang, J. Supramolecular-Templated Thick Mesoporous Titania Films for Dye-Sensitized Solar Cells: Effect of Morphology on Performance. *ACS Appl. Mater. Interfaces* **2009**, *1*, 2789−2795.

(11) Patrocinio, A. O. T.; Mizoguchi, S. K.; Paterno, L. G.; Garcia, C. G.; Murakami Iha, N. Y. Efficient and Low Cost Devices for Solar Energy Conversion: Efficiency and Stability of Some Natural-Dye-Sensitized Solar Cells. *Synth. Met.* **2009**, *159*, 2342−2344.

(12) Procházka, J.; Kavan, L.; Zukalová, M.; Frank, O.; Kalbáč, M.; Zukal, A.; Klementová, M.; Carbone, D.; Graetzel, M. Novel Synthesis of the TiO_2(B) Multilayer Templated Films. *Chem. Mater.* **2009**, *21*, 1457−1464.

(13) Kroon, J. M.; Bakker, N. J.; Smit, H. J. P.; Liska, P.; Thampi, K. R.; Wang, P.; Zakeeruddin, S. M.; Grätzel, M.; Hinsch, A.; Hore, S.; Würfel, U.; Sastrawan, R.; Durrant, J. R.; Palomares, E.; Pettersson, H.; Gruszecki, T.; Walter, J.; Skupien, K.; Tulloch, G. E. Nanocrystalline Dye-Sensitized Solar Cells Having Maximum Performance. *Progress in Photovoltaics: Research and Applications* **2007**, *15*, 1−18.

(14) Argazzi, R.; Murakami Iha, N. Y.; Zabri, H.; Odobel, F.; Bignozzi, C. A. Design of Molecular Dyes for Application in Photoelectrochemical and Electrochromic Devices Based on Nanocrystalline Metal Oxide Semiconductors. *Coord. Chem. Rev.* **2004**, *248*, 1299−1316.

(15) Wang, P.; Zakeeruddin, S. M.; Comte, P.; Charvet, R.; Humphry-Baker, R.; Grätzel, M. Enhance the Performance of Dye-Sensitized Solar Cells by Co-grafting Amphiphilic Sensitizer and Hexadecylmalonic Acid on TiO_2 Nanocrystals. *J. Phys. Chem. B* **2003**, *107*, 14336−14341.

(16) Garcia, C. G.; Polo, A. S.; Murakami Iha, N. Y. Fruit Extracts and Ruthenium Polypyridinic Dyes for Sensitization of TiO_2 in Photoelectrochemical Solar Cells. *J. Photochem. Photobiol., A* **2003**, *160*, 87−91.

(17) Nazeeruddin, M. K.; Kay, A.; Rodicio, I.; Humphry-Baker, R.; Mueller, E.; Liska, P.; Vlachopoulos, N.; Graetzel, M. Conversion of Light to Electricity by cis-X_2bis(2,2′-bipyridyl-4,4′-dicarboxylate)-ruthenium(II) Charge-Transfer Sensitizers (X = Cl^-, Br^-, I^-, CN^-, and SCN^-) on Nanocrystalline Titanium Dioxide Electrodes. *J. Am. Chem. Soc.* **1993**, *115*, 6382−6390.

(18) O'Regan, B.; Grätzel, M. A Low-Cost, High-Efficiency Solar Cell Based on Dye-Sensitized Colloidal TiO_2 Films. *Nature* **1991**, *353*, 737−740.
(19) Zhao, Y.; Zhai, J.; He, J.; Chen, X.; Chen, L.; Zhang, L.; Tian, Y.; Jiang, L.; Zhu, D. High-Performance All-Solid-State Dye-Sensitized Solar Cells Utilizing Imidazolium-Type Ionic Crystal as Charge Transfer Layer. *Chem. Mater.* **2008**, *20*, 6022−6028.
(20) Peter, L. M. Characterization and Modeling of Dye-Sensitized Solar Cells. *J. Phys. Chem. C* **2007**, *111*, 6601−6612.
(21) Peter, L. Transport, Trapping and Interfacial Transfer of Electrons in Dye-Sensitized Nanocrystalline Solar Cells. *J. Electroanal. Chem.* **2007**, *599*, 233−240.
(22) Cameron, P. J.; Peter, L. M.; Hore, S. How Important is the Back Reaction of Electrons via the Substrate in Dye-Sensitized Nanocrystalline Solar Cells. *J. Phys. Chem. B* **2005**, *109*, 930−936.
(23) Cameron, P. J.; Peter, L. M. Characterization of Titanium Dioxide Blocking Layers in Dye-Sensitized Nanocrystalline Solar Cells. *J. Phys. Chem. B* **2003**, *107*, 14394−14400.
(24) Krüger, J.; Plass, R.; Grätzel, M.; Cameron, P. J.; Peter, L. M. Charge Transport and Back Reaction in Solid-State Dye-Sensitized Solar Cells: A Study Using Intensity-Modulated Photovoltage and Photocurrent Spectroscopy. *J. Phys. Chem. B* **2003**, *107*, 7536−7539.
(25) Palomares, E.; Clifford, J. N.; Haque, S. A.; Lutz, T.; Durrant, J. R. Control of Charge Recombination Dynamics in Dye Sensitized Solar Cells by the Use of Conformally Deposited Metal Oxide Blocking Layers. *J. Am. Chem. Soc.* **2003**, *125*, 475−482.
(26) Xia, J.; Masaki, N.; Jiang, K.; Wada, Y.; Yanagida, S. Importance of Blocking Layers at Conducting Glass/TiO_2 Interfaces in Dye-Sensitized Ionic-Liquid Solar Cells. *Chem. Lett.* **2006**, *35*, 252−253.
(27) Ito, S.; Liska, P.; Comte, P.; Charvet, R.; Pechy, P.; Bach, U.; Schmidt-Mende, L.; Zakeeruddin, S. M.; Kay, A.; Nazeeruddin, M. K.; Gratzel, M. Control of Dark Current in Photoelectrochemical (TiO_2/I^--I^{3-}) and Dye-Sensitized Solar Cells. *Chem. Commun.* **2005**, 4351−4353.
(28) Paula, L. F.; Amaral, R. C.; Murakami Iha, N. Y.; Paniago, R. M.; Machado, A. E. H.; Patrocinio, A. O. T. New Layer-by-Layer Nb_2O_5-TiO_2 Film as an Effective Underlayer in Dye-Sensitised Solar Cells. *RSC Adv.* **2014**, *4*, 10310−10316.
(29) Choi, H.; Nahm, C.; Kim, J.; Moon, J.; Nam, S.; Jung, D.-R.; Park, B. The Effect of $TiCl_4$-Treated TiO_2 Compact Layer on the Performance of Dye-Sensitized Solar Cell. *Curr. Appl. Phys.* **2012**, *12*, 737−741.
(30) Patrocinio, A. O. T.; El-Bacha, A. S.; Paniago, E. B.; Paniago, R. M.; Murakami Iha, N. Y. Influence of the Sol-Gel pH Process and Compact Film on the Efficiency of TiO_2-Based Dye-Sensitized Solar Cells. *Int. J. Photoenergy* **2012**, *2012*, Article 638571.
(31) Liu, Y.; Sun, X.; Tai, Q.; Hu, H.; Chen, B.; Huang, N.; Sebo, B.; Zhao, X.-Z. Influences on Photovoltage Performance by Interfacial Modification of FTO/Mesoporous TiO_2 Using ZnO and TiO_2 as the Compact Film. *J. Alloys Compd.* **2011**, *509*, 9264−9270.
(32) Cho, T.-Y.; Yoon, S.-G.; Sekhon, S. S.; Kang, M. G.; Han, C.-H. The Effect of a Sol-gel Formed TiO_2 Blocking Layer on the Efficiency of Dye-Sensitized Solar Cells. *Bull. Korean Chem. Soc.* **2011**, *32*, 3629−3633.
(33) Patrocinio, A. O. T.; Paterno, L. G.; Murakami Iha, N. Y. Role of Polyelectrolyte for Layer-by-Layer Compact TiO_2 Films in Efficiency Enhanced Dye-Sensitized Solar Cells. *J. Phys. Chem. C* **2010**, *114*, 17954−17959.
(34) Patrocinio, A. O. T.; Paterno, L. G.; Murakami Iha, N. Y. Layer-by-Layer TiO_2 Films as Efficient Blocking Layers in Dye-Sensitized Solar Cells. *J. Photochem. Photobiol., A* **2009**, *205*, 23−27.
(35) Yu, H.; Zhang, S.; Zhao, H.; Will, G.; Liu, P. An Efficient and Low-Cost TiO_2 Compact Layer for Performance Improvement of Dye-Sensitized Solar Cells. *Electrochim. Acta* **2009**, *54*, 1319−1324.
(36) Handa, S.; Haque, S. A.; Durrant, J. R. Saccharide Blocking Layers in Solid State Dye Sensitized Solar Cells. *Adv. Funct. Mater.* **2007**, *17*, 2878−2883.
(37) Hart, J. N.; Menzies, D.; Cheng, Y.-B.; Simon, G. P.; Spiccia, L. TiO_2 Sol−Gel Blocking Layers for Dye-Sensitized Solar Cells. *C. R. Chim.* **2006**, *9*, 622−626.
(38) Sommeling, P. M.; O'Regan, B. C.; Haswell, R. R.; Smit, H. J. P.; Bakker, N. J.; Smits, J. J. T.; Kroon, J. M.; Van Roosmalen, J. A. M. Influence of a $TiCl_4$ Post-Treatment on Nanocrystalline TiO_2 Films in Dye-Sensitized Solar Cells. *J. Phys. Chem. B* **2006**, *110*, 19191−19197.
(39) Xia, J.; Masaki, N.; Jiang, K.; Yanagida, S. Deposition of a Thin Film of TiO_x from a Titanium Metal Target as Novel Blocking Layers at Conducting Glass/TiO_2 Interfaces in Ionic Liquid Mesoscopic TiO_2 Dye-Sensitized Solar Cells. *J. Phys. Chem. B* **2006**, *110*, 25222−25228.
(40) Barbé, C. J.; Arendse, F.; Comte, P.; Jirousek, M.; Lenzmann, F.; Shklover, V.; Grätzel, M. Nanocrystalline Titanium Oxide Electrodes for Photovoltaic Applications. *J. Am. Ceram. Soc.* **1997**, *80*, 3157−3171.
(41) Yuan, S.; Mu, J.; Mao, R.; Li, Y.; Zhang, Q.; Wang, H. All-Nanoparticle Self Assembly ZnO/TiO_2 Heterojunction Thin Films with Remarkably Enhanced Photoelectrochemical Activity. *ACS Appl. Mater. Interfaces* **2014**, *6*, 5719−5725.
(42) Paterno, L.; Soler, M. G. Layer-by-Layer Enabled Nanomaterials for Chemical Sensing and Energy Conversion. *JOM* **2013**, *65*, 709−719.
(43) Decher, G. Fuzzy Nanoassemblies: Toward Layered Polymeric Multicomposites. *Science* **1997**, *277*, 1232−1237.
(44) Patrocinio, A. O. T.; Paniago, E. B.; Paniago, R. M.; Murakami Iha, N. Y. XPS Characterization of Sensitized n-TiO_2 Thin Films for Dye-Sensitized Solar Cell Applications. *Appl. Surf. Sci.* **2008**, *254*, 1874−1879.
(45) Murakami Iha, N. Y.; Garcia, C. G.; Bignozzi, C. A. In *Handbook of Photochemistry and Photobiology*; Nalwa, H. S., Eds.; American Scientific Publishers: Stevenson Ranch, CA, 2003; Chapter 2, pp 49−75.
(46) Polo, A. S.; Murakami Iha, N. Y. Blue Sensitizers for Solar Cells: Natural Dyes from Calafate and Jaboticaba. *Sol. Energy Mater. Sol. Cells* **2006**, *90*, 1936−1944.
(47) Chen, X.; Mao, S. S. Titanium Dioxide Nanomaterials: Synthesis, Properties, Modifications, and Applications. *Chem. Rev.* **2007**, *107*, 2891−2959.
(48) Diebold, U. The Surface Science of Titanium Dioxide. *Surf. Sci. Rep.* **2003**, *48*, 53−229.
(49) Bedja, I.; Kamat, P. V.; Hua, X.; Lappin, A. G.; Hotchandani, S. Photosensitization of Nanocrystalline ZnO Films by Bis(2,2′-bipyridine)(2,2′-bipyridine-4,4′-dicarboxylic acid)ruthenium(II). *Langmuir* **1997**, *13*, 2398−2403.
(50) Zaban, A.; Greenshtein, M.; Bisquert, J. Determination of the Electron Lifetime in Nanocrystalline Dye Solar Cells by Open-Circuit Voltage Decay Measurements. *ChemPhysChem* **2003**, *4*, 859−864.
(51) Bisquert, J.; Grätzel, M.; Wang, Q.; Fabregat-Santiago, F. Three-Channel Transmission Line Impedance Model for Mesoscopic Oxide Electrodes Functionalized with a Conductive Coating. *J. Phys. Chem. B* **2006**, *110*, 11284−11290.
(52) Bisquert, J. Theory of the Impedance of Electron Diffusion and Recombination in a Thin Layer. *J. Phys. Chem. B* **2002**, *106*, 325−333.
(53) Fabregat-Santiago, F.; Garcia-Belmonte, G.; Bisquert, J.; Zaban, A.; Salvador, P. Decoupling of Transport, Charge Storage, and Interfacial Charge Transfer in the Nanocrystalline TiO_2/Electrolyte System by Impedance Methods. *J. Phys. Chem. B* **2002**, *106*, 334−339.